

CALPHAD Modeling and Microstructure Investigation of Mg–Gd–Y–Zn Alloys

Janet Meier, Josh Caris, and Alan A. Luo

Abstract

In this study, CALPHAD (CALculation of PHase Diagrams) modeling was used to design and optimize Mg–Gd–Y–Zn alloys containing long period stacking order (LPSO) phases. The selected compositions were evaluated using scanning electron microscopy, energy dispersive spectroscopy, and X-ray diffraction to identify major phases and determine their area fractions. It was seen in as-cast samples that a blocky LPSO 14H phase formed at the grain boundaries while a filament-type LPSO 14H formed in the Mg grains. As the rare earth (RE) and Zn concentrations increased, eutectic Zn-rich intermetallics and more of the RE-rich blocky LPSO formed along grain boundaries. After annealing, an increase in the Zn-rich intermetallic area fraction, decrease in bulky LPSO area fraction, and increase in filament-type LPSO were observed. In higher alloyed samples, a Zn- and Y-rich phase was observed that was not consistent with the predicted or reported phase. These results indicate the present CALPHAD databases well represent the LPSO 14H formation in the Mg–Gd–Y–Zn system studied and can be used to tailor the microstructure to potentially improve the strength and ductility in these alloys. Further investigation is needed to determine if the existing reliably databases model the other secondary phases.

Keywords

Long period stacking order (LPSO) • Microstructure • Magnesium alloys • CALPHAD • Alloy development

J. Meier · A. A. Luo (✉)
The Ohio State University, Columbus, OH, USA
e-mail: luo.445@osu.edu

J. Caris
Terves LLC, Euclid, OH, USA

Introduction

As magnesium alloys become more widely used in structural applications, there is a growing need for improvements in strength and ductility for these alloys. In recent years, such improvements in properties have been found in alloys containing long period stacking ordered (LPSO) phases [1–4]. LPSO phases can form in Mg alloys that contain a smaller atomic radius transition metal, such as Zn, and larger rare earth elements (RE), such as Y and Gd, due to the reduction in stacking fault energy caused by these alloying elements [5–8]. The RE and Zn atoms cluster along the basal plane to form enriched layers [9]. These layers form building blocks with a local face centered cubic structure that is bounded by Shockley partial dislocations [9]. The spacing and combination of these building blocks with the Mg lattice produce several different LPSO structures, where the most frequently observed are 14H and 18R. The difference between the two phases is the number of Mg layers between the building blocks: LPSO 14H has three layers and 18R has two [9, 10].

The LPSO phase in Mg alloys forms in two major morphologies, depending on composition and thermomechanical processing [8, 11–17]. The first morphology is a blocky phase found at the grain boundaries. As the volume fraction of LPSO increases, the blocky phase forms a network around the α -Mg grains. The second morphology is a fine lamellar phase located in the α -Mg grains. Improved strength and ductility in LPSO-containing alloys come from the impedence of dislocation motion and twin formation by the relatively thick LPSO phases [8, 10, 13, 16, 18]. The LPSO structure increases the critical resolve shear stress for basal and prismatic slip, which provides strengthening and activates slip in other grains to improve ductility [11, 19]. As a result, maximizing the phase fraction of LPSO could greatly improve the mechanical properties of Mg alloys.

Previous researchers have developed criteria for the critical ratio of RE to Zn to produce LPSO phases, but as the alloy systems become more complex it is more difficult to

predict the resulting microstructures. A CALPHAD (CALculation of PHase Diagrams)-based approach [20] provides an opportunity to quantitatively predict the phase composition of these more complex alloys. In this work, the available databases for two CALPHAD software packages, Thermo-Calc and PANDAT, were evaluated to predict the phases of three Mg–Gd–Y–Zn alloys, followed by experimental validation.

Modeling and Experimental Methods

Equilibrium and Scheil calculations were conducted using Thermo-Calc and PANDAT for several compositions in the Mg–Gd–Y–Zn system to assess the predicted phase fractions of LPSO and intermetallic phases. Three compositions, shown in Table 1, were selected and cast for microstructural analysis.

The alloys were prepared and cast by Terves LLC. The raw materials (commercially pure Mg, Zn, Gd, and Y) were melted in a 75 lb gas fired furnace with a pneumatic shear mixer. A CO₂ and SF₆ gas mixture was used as a cover gas in the furnace and applied to the mold riser to prevent oxidation of the melt. The samples were cast into a 7" × 7" × 4" steel permanent mold. The castings were then sectioned, annealed at 500° for 9 h and water quenched, and mounted in Bakelite for scanning electron microscope (SEM) analysis. Final alloy compositions (Table 1) were determined using a combination of inductively coupled plasma mass spectroscopy (ICP) and spark optical emission spectroscopy (OES).

Samples were ground and polished to 0.05 μm colloidal silica, and SEM analysis was performed using a FEI Apreo FEG microscope with EDAX Octane Elect energy dispersive spectroscopy (EDS) capabilities. EDS spot and mapping analysis was performed using a TEAM software.

Table 1 Compositions of the three samples used in this study (determined using ICP and OES)

Sample	Mg (wt%)	Gd (wt%)	Y (wt%)	Zn (wt%)
MC07	82.98	10.4	3.62	3.00
MC14	81.73	10.57	5.25	2.45
MC21	79.95	10.2	4.74	5.1

Table 2 Existing ternary systems and LPSO phases present in the Thermo-Calc TCMG5 and PANDAT PanMg2018_TH + MB databases

	Thermo-calc	PANDAT
Ternary systems	Mg–Gd–Y Mg–Gd–Zn Mg–Y–Zn	Mg–Gd–Y Mg–Gd–Zn Mg–Y–Zn
LPSO phases	LPSO_14H LPSO_18R	LPSO_14H LPSO_18R LPSO_10H

The area fraction of each phase was determined from ten images from each sample using ImageJ. The samples were then removed from the Bakelite mounts and polished to 1200 grit for X-ray diffraction (XRD) analysis. A Rigaku MiniFlex 600 system with a Cu source and Ni filter set to 40 kV and 15 mA was used for phase identifications. The Rigaku PDXL 2 software and literature data were used to identify the XRD peaks.

Results and Discussion

CALPHAD Modeling

In order to appropriately model a multicomponent alloy system with CALPHAD, there must be a reliable database that represents all related binary and ternary systems. The ternary systems included in the Thermo-Calc and PANDAT databases are listed in Table 2. Both systems contain data for the three ternary systems for the Mg rich corner, but PANDAT also has the LPSO 10H phase defined in their database. It should be noted that although both programs contain data for the same ternary systems, they may be using different datasets or computational methods. As a result, there will likely be variations in the predicted results.

For each alloy, both equilibrium and Scheil calculations were performed to represent the two extremes seen in cast alloys. The Scheil calculation represents rapid cooling during solidification, where diffusion can occur in the liquid but not the solid. On the other hand, the equilibrium calculation better represents alloys with very slow cooling during solidification or after annealing heat treatment. The predicted phases for the three alloys studied in this work can be seen in Fig. 1.

For the compositional range, there were a total of seven predicted phases between the two programs. The primary

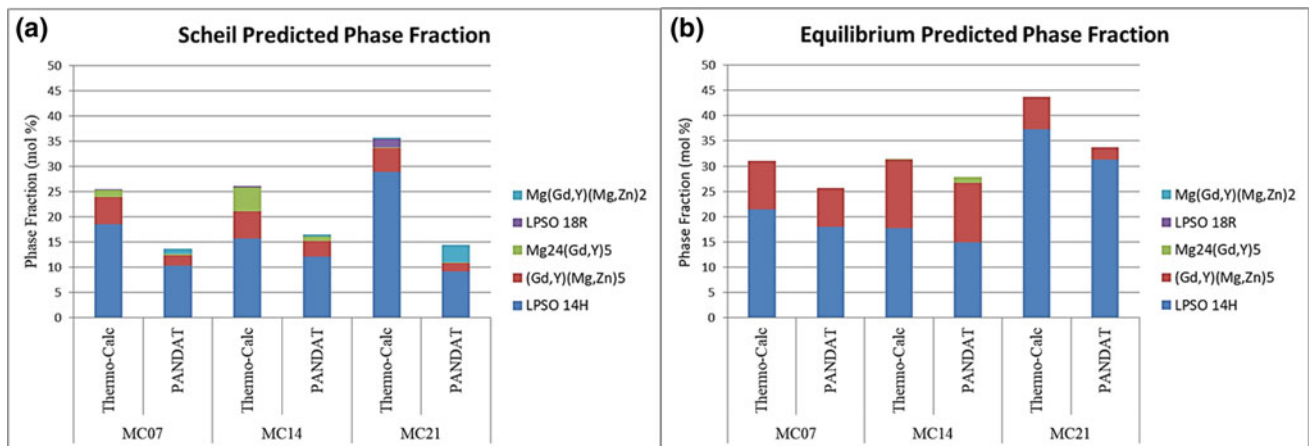


Fig. 1 Predicted phases and mole fractions of each phase in the (a) Scheil and (b) equilibrium conditions

phase predicted for all compositions was the hexagonal close packed (hcp) Mg matrix, as expected. In the case of the LPSO phases, both programs predicted the presence of the LPSO 14H phase. The LPSO 14H phase has been reported as a very stable phase that can form both at the grain boundaries and in the primary Mg grains [8, 11–17]. Also, the LPSO 14H phase has been reported to transform from other phases, and intragranular growth is driven by the diffusion of Zn and the RE [8–12, 15, 16]. The increase in the mole fraction of LPSO 14H between the Scheil and equilibrium conditions predicted by both programs is consistent with these previous findings.

Thermo-Calc also predicted 0.34 and 1.7 mol% of the LPSO 18R for MC14 and MC21 samples, respectively, in the Scheil condition (Fig. 1). In the equilibrium condition, no LPSO 18R is predicted. Previous studies have found that LPSO 18R forms at the grain boundaries during solidification in Mg–Y–Zn and Mg–Gd–Y–Zn alloys [8, 21–23]. The LPSO 18R transforms into 14H during annealing, and both phases can exist simultaneously in the same grain [19]. Due to the low predicted fractions and the deviations from the Scheil condition seen in the as-cast samples, the LPSO 18R phase may not be observable in this study.

PANDAT predicts a phase called RM3_W in the Scheil condition for all three alloys that is defined as $Mg_{0.25}(Gd, Y)_{0.25}(Mg, Zn)_{0.5}$. Thermo-Calc also predicts a similar phase called L12_RMZGN2, defined as $Mg_1(Gd, Y)_1(Mg, Zn)_2$, for the MC21 alloy in the Scheil condition. For similar compositions, there has been a reported $Mg_3(Gd, Y)$ phase [12, 17, 24–26] and a reported $W-Mg_3Y_2Zn_3$ phase [8, 15, 17, 27, 28]. In their 2018 paper, Luo et al. discussed that the $W-Mg_3Y_2Zn_3$ phase had been misidentified as $Mg_3(Gd, Y)$ in past studies [16]. Neither Thermo-Calc or PANDAT has the $W-Mg_3Y_2Zn_3$ phase in their databases, so it is possible that these phases were not separately identified in either program. For this study, the predicted mole fractions of the RM3_W

and L12_RMZGN2 phases are predicted in low amounts in the Scheil condition and are not predicted in the equilibrium condition (Fig. 1). As a result, they may not be observable in this study. Future work will be needed to evaluate these two phases in the databases.

In the Scheil and equilibrium conditions, both programs predict the presence of a $(Mg, Zn)_5(Gd, Y)$ phase. This phase is generally reported as the β phase and has been observed in a wide range of LPSO-forming alloys [10, 11, 16, 24, 25, 29]. The mole fraction of $(Mg, Zn)_5(Gd, Y)$ is predicted to increase between the Scheil and equilibrium conditions, which is consistent with proposed precipitation sequences that have $(Mg, Zn)_5(Gd, Y)$ as an equilibrium phase [26]. The final predicted phase is $Mg_{24}(Gd, Y)_5$. Both programs predict small mole fractions of this phase in the Scheil condition and in the equilibrium condition for MC14. $Mg_{24}(Gd, Y)_5$ has also been reported as the β phase in some studies [8, 12, 25], as a result the two phases will be referred to by their compositions in this work. The $Mg_{24}(Gd, Y)_5$ phase has been observed in Mg–Gd–Zn–Zr and Mg–Y–Zn–Zr alloys, but is predicted at relatively low mole fractions in the present alloys.

The predicted mole fractions for each phase at the end of solidification for the Scheil model and at room temperature for equilibrium model were calculated in both programs (Fig. 1). For the LPSO 14H phase, Thermo-Calc consistently predicts a higher mole fraction. This is also true for the $(Mg, Zn)_5(Gd, Y)$ phase. For the Scheil model, which more closely represents the as-cast state, Thermo-Calc also predicts a higher mole fraction of the $Mg_{24}(Gd, Y)_5$ phase for the three compositions. In the equilibrium calculation, which more closely represents the annealed state, only MC14 is predicted to have the $Mg_{24}(Gd, Y)_5$ phase, and PANDAT predicts a larger mole fraction. The mole fraction of LPSO is predicted by both programs to increase with annealing. This prediction is consistent with the expected diffusion of RE and Zn during annealing reported in literature [9, 16].

There is also a predicted increase in the mole fraction of the $(\text{Mg,Zn})_5(\text{Gd,Y})$ phase with annealing as well.

Microstructural Analysis

The microstructure from SEM of the as-cast and annealed samples can be seen in Fig. 2. The T1 detector used acts similar to a backscatter detector and collects the high-energy,

low-angle electrons. As a result, Z-contrast can be used to help identify phases. The dark, background phase was identified as the primary Mg grains using EDS spot and mapping analysis. Dark spots seen in the Mg grains, particularly in the as-cast samples, are believed to be corrosion pits formed during sample preparation. In all the samples, there is a small amount of a small, bright rectangular phase. Upon EDS analysis, there were high Y and O signals, which are most likely yttrium oxide formed during the casting process.

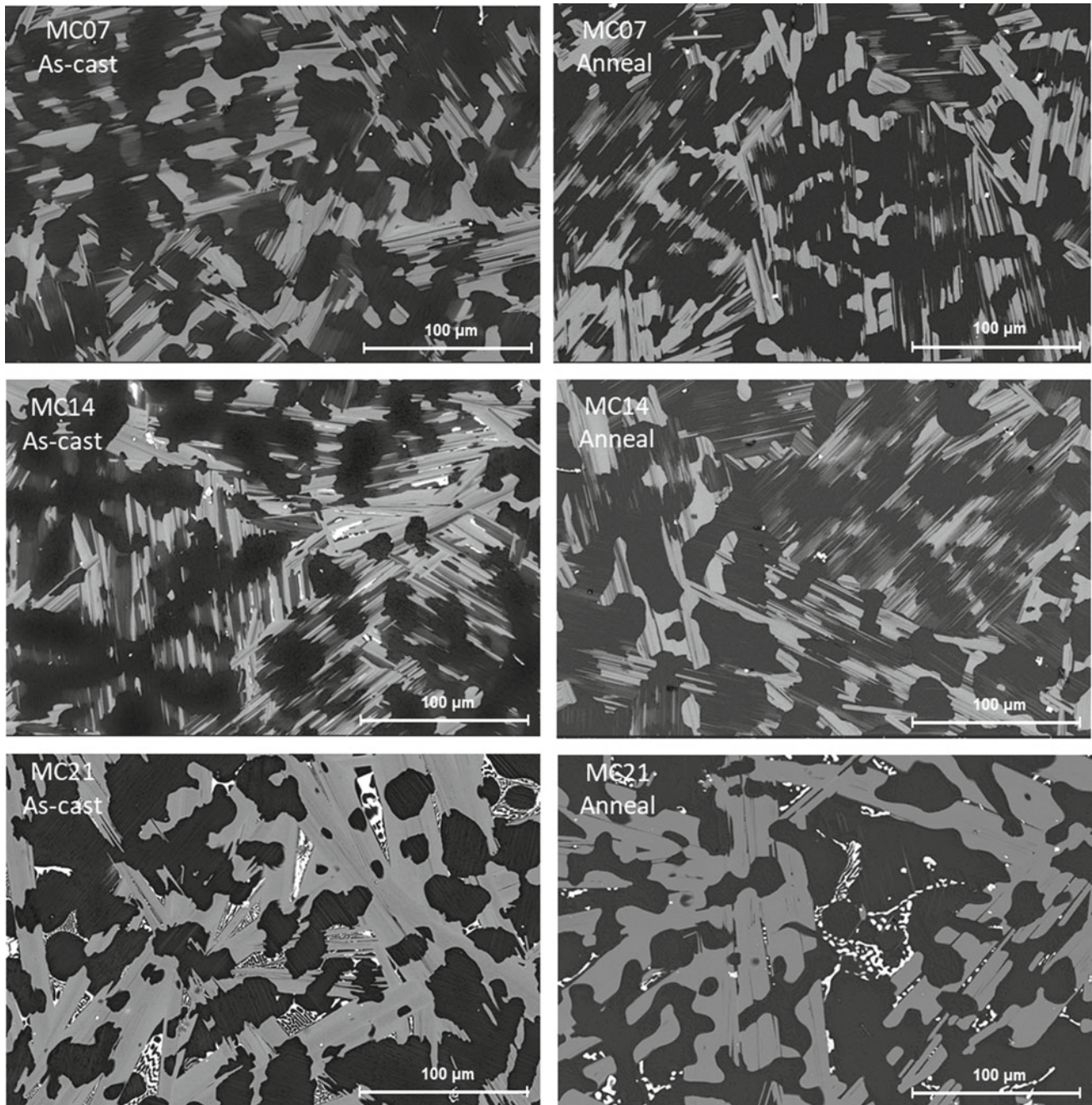


Fig. 2 SEM images using a T1 (backscatter-like) detector for the as-cast and annealed conditions

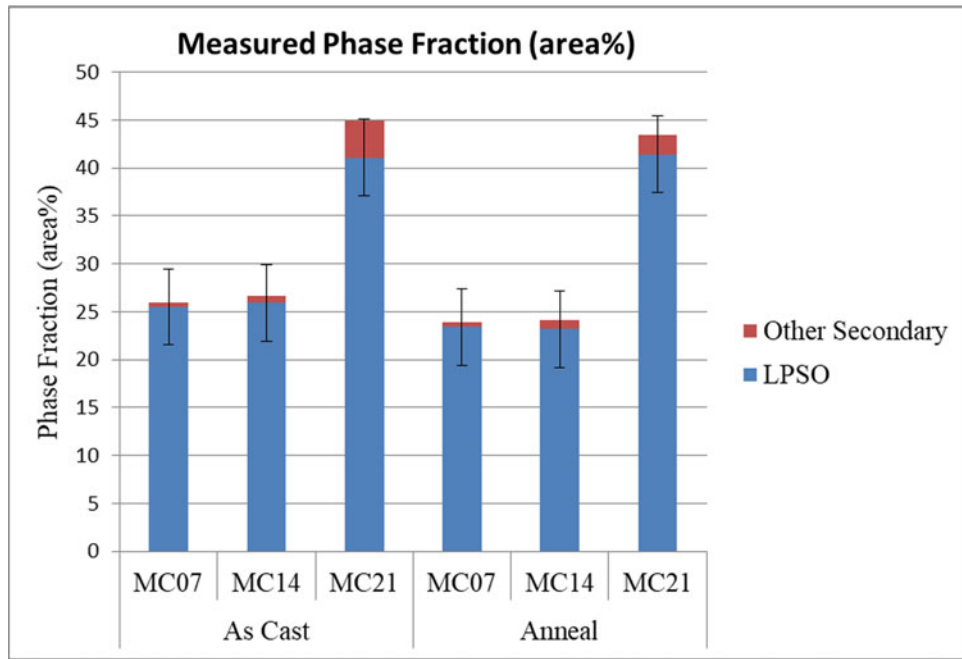


Fig. 3 Measured area fractions of the LPSO 14H and other secondary phases in the as-cast and annealed conditions

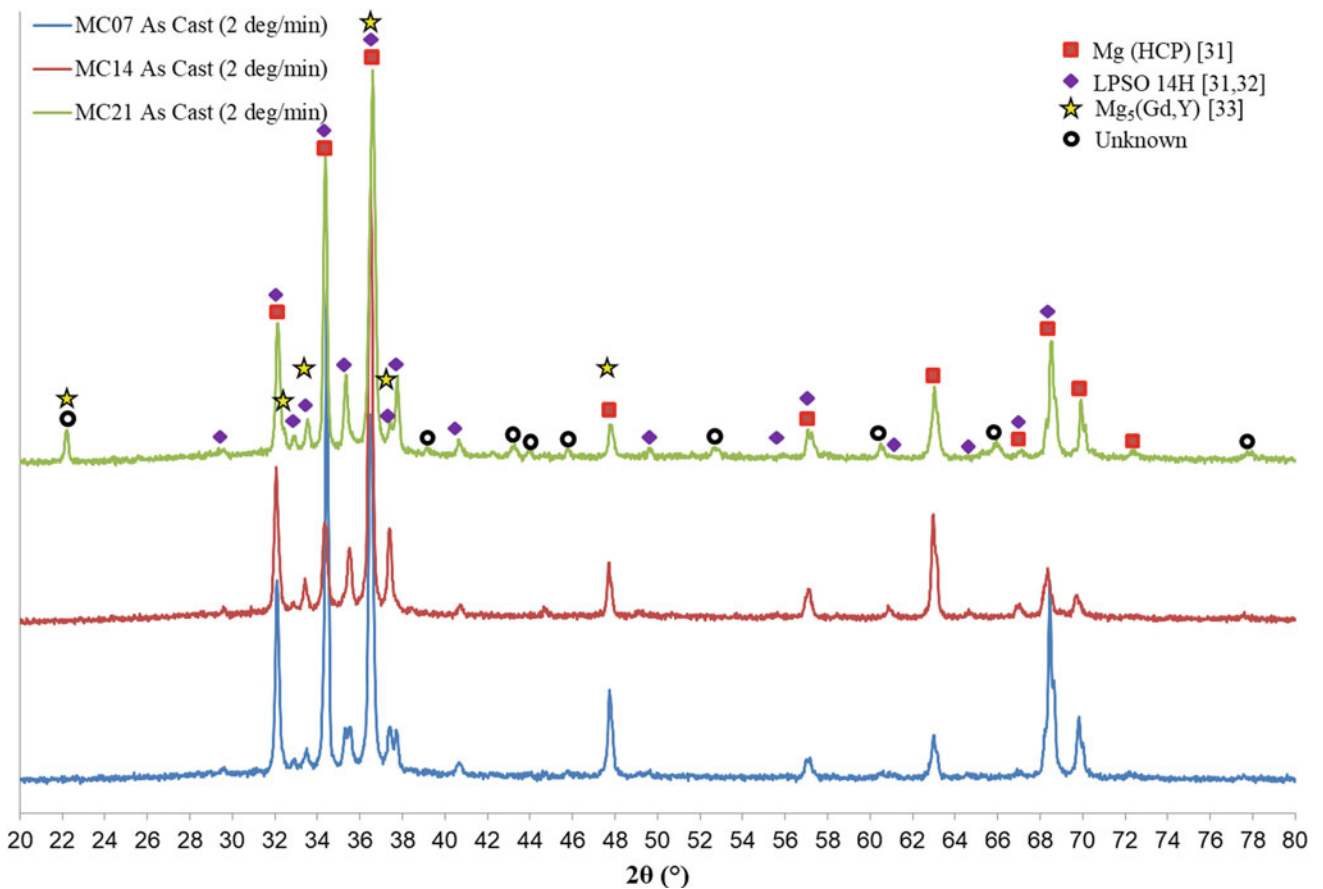


Fig. 4 XRD analysis of the as-cast samples

The high area fraction medium grey phase seen in all of the samples has a blocky morphology that becomes more lamellar with annealing. EDS mapping of this phase indicates it has a higher Y and Zn signal than the Mg matrix. As the Gd concentration increases, EDS mapping shows that the relative Gd concentration in the medium grey phase also increases. This is due to the lower solubility of Y and Zn in Mg and the higher solubility of Gd in Mg [30]. The area fraction of the phase also increases with increased alloying, with MC21 showing the largest area fraction of this phase (Fig. 3). Based on the CALPHAD predictions, this phase is most likely the LPSO 14H phase. This is supported by XRD analysis (Figs. 4 and 5), which has Mg and the LPSO 14H as the dominant phases.

After annealing, there is a small reduction in the measured ω LPSO 14H area fraction (Fig. 3). One explanation for this could be the formation of lamellar LPSO 14H in the Mg grains that is not easily observable at the magnification used for volume fraction measurements. At higher magnification, small bright lamellar features can be seen extending from the grain boundaries into the Mg matrix (Fig. 6). This phase is in one orientation in each grain. The presence of this

lamellar phase increases with increased alloying and with annealing, with the possible exception of the MC21 sample. This phase is most likely LPSO 14H, and the increase in its formation after annealing is consistent with the diffusion of RE and Zn from the grain boundaries into the grains, as reported in literature [8, 12–17, 27, 31]. As a result, there is a decrease in the area fraction of bulky LPSO 14H at the grain boundaries.

In the as-cast MC14 and MC21 samples, there is a bright phase along the grain boundaries (Figs. 2 and 6). In the MC21 sample, this phase has a eutectic morphology and increases in area fraction in comparison with the lower alloy MC14 sample. With annealing, the area fraction of the bright phase is reduced in MC21 and is no longer observable in MC14. Based on the CALPHAD analysis, this bright phase is most likely $(\text{Mg,Zn})_5(\text{Gd,Y})$ or $\text{Mg}_{24}(\text{Gd,Y})_5$ due to predicted mole fraction. EDS mapping of this phase indicates there are relatively high Zn and Y concentrations and no presence of Mg and Gd. In the as-cast MC14 sample, there was some Gd signal in the EDS map for the bright phase. Based on the high Zn content, this phase is unlikely to be $\text{Mg}_{24}(\text{Gd,Y})_5$. XRD analysis (Figs. 4 and 5) indicates that

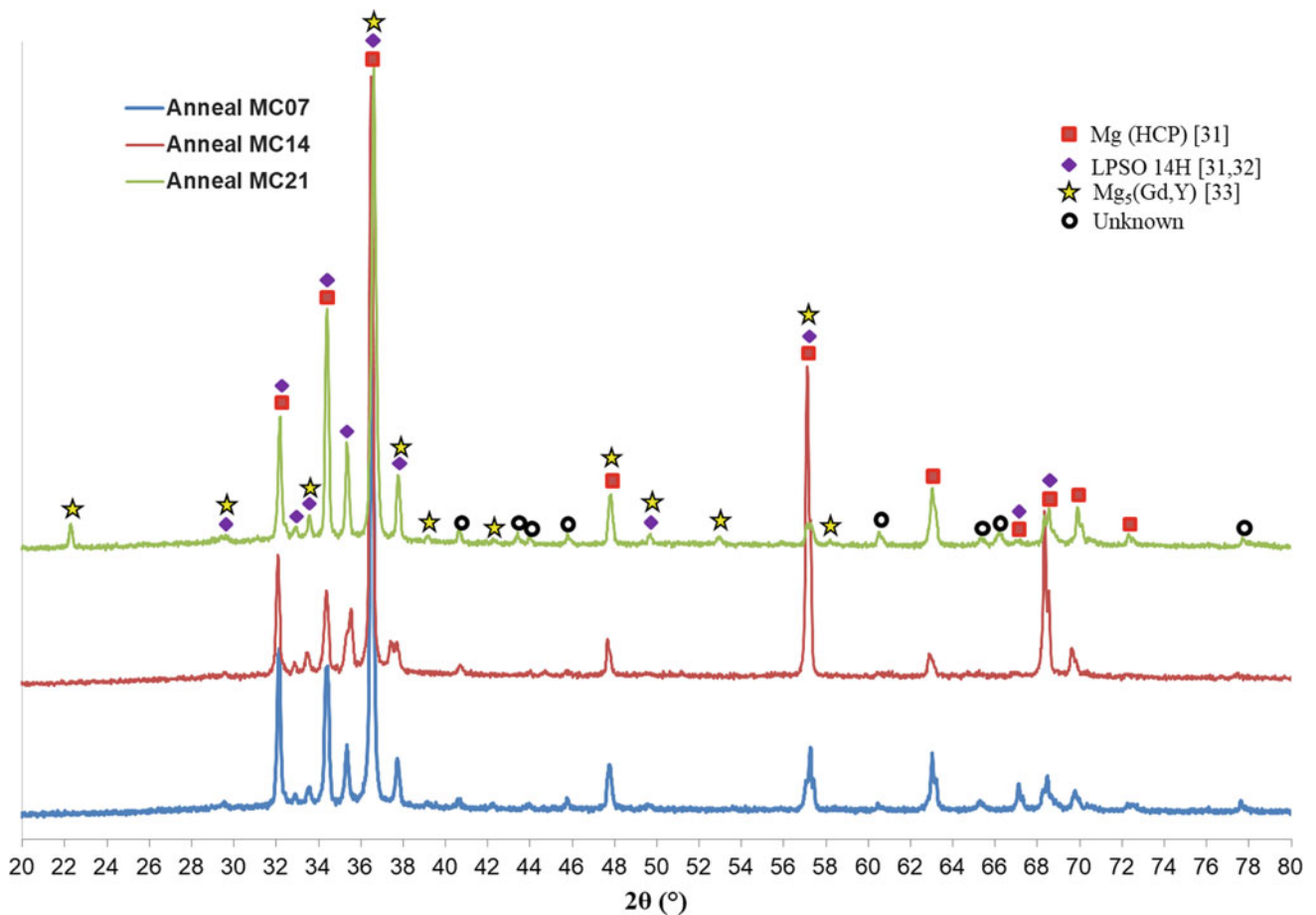


Fig. 5 XRD analysis of the annealed samples

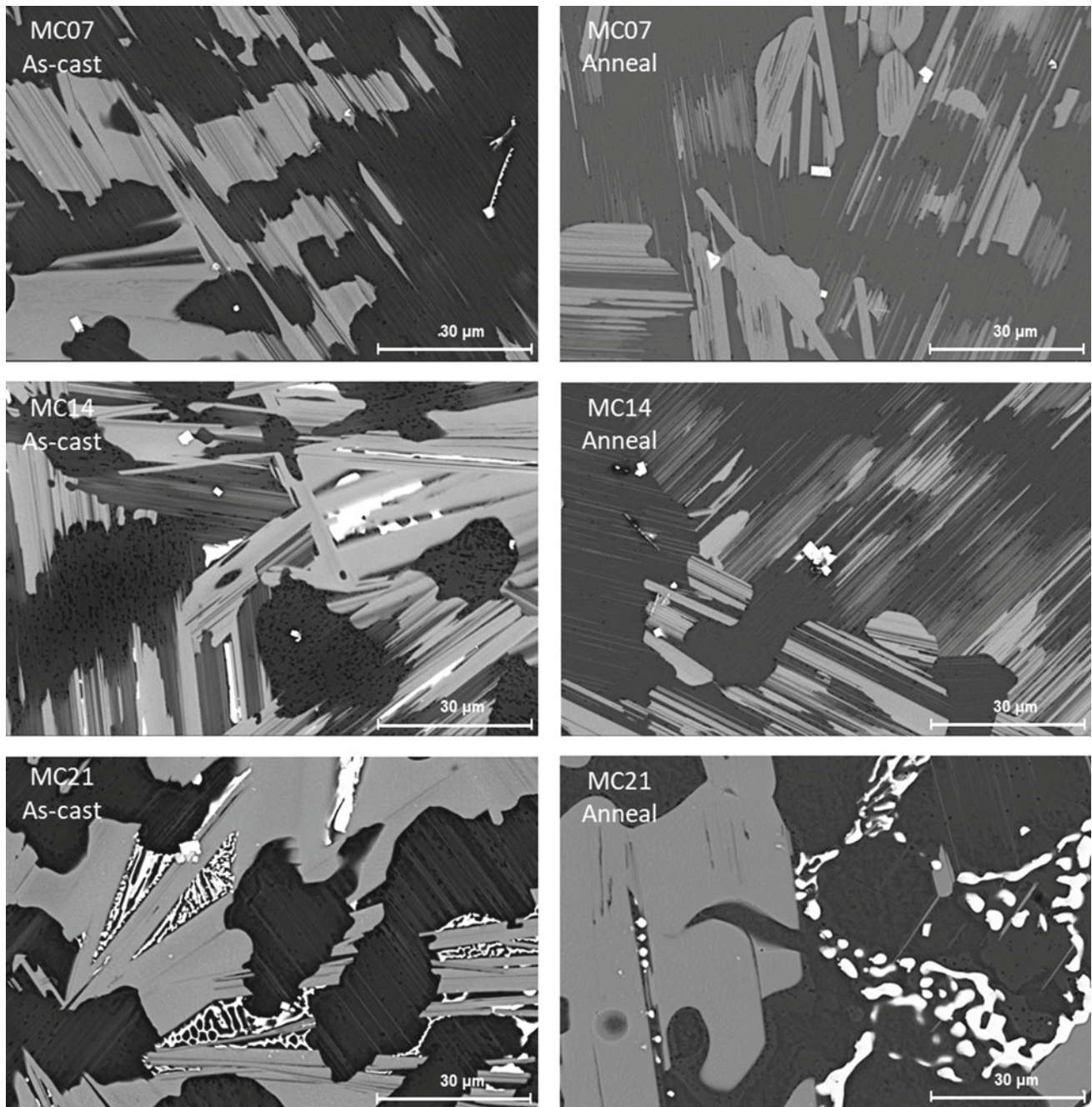


Fig. 6 SEM images using a T1 (backscatter-like) detector for the as-cast and annealed conditions

$Mg_{24}(Gd,Y)_5$ and $W-Mg_3Y_2Zn_3$ were either not present in the alloys or not in large enough quantities to be observed. Looking more closely at the CALPHAD predictions, the $(Mg,Zn)_5(Gd,Y)$ phase has a composition consistent with Mg_5Gd , so it is unlikely to be the bright phase in the SEM images. At this point, literature has not reported a Zn-Y binary phase, and further analysis is needed for phase identification.

For the LPSO 14H phase, the existing CALPHAD databases evaluated in this study predict a high phase fraction that is reasonable. The predicted increase of the LPSO 14H phase with increased alloying and annealing was consistent with both literature and microstructural analysis. In terms of the other intermetallic phases, the predictive capabilities of the model were less reliable. Part of this is due to the lower predicted phase fraction of the intermetallics and partly due

to the phase definitions in the database. The biggest discrepancy is the prediction of the Mg₅Gd phase and the presence of a Zn- and Y-rich intermetallic phase in the MC14 and MC21 samples. As a result, it was determined that the existing CALPHAD databases evaluated in this study can represent the LPSO 14H phase, but more evaluation is needed for the other secondary intermetallic phases.

Conclusions

The existing databases for two CALPHAD programs, PANDAT and Thermo-Calc, were evaluated for their predictive capabilities for LPSO-forming alloys in the Mg–Gd–Y–Zn system. Three compositions were examined in the as-cast and annealed conditions using SEM, EDS, and XRD analysis. It was shown that the CALPHAD programs reasonably predicted the presence of the LPSO 14H phase in these alloys. The other phases predicted by the programs were consistent with phases previously observed in the literature. The phases predicted by both programs were generally consistent with each other, although the mole fractions of these phases were different. Unlike the LPSO 14H phase, the other predicted phases were not observed during SEM analysis. This is possibly due to low phase fractions for these phases. Query ID="Q4" Text="Please check whether the edits made in the sentence ‘...with either the predicted phases or reported phases’ convey the intended meaning.’ In the higher alloy samples, there was a Zn- and Y-rich phase that was not consistent with either the predicted phases or reported phases. Based on these findings, it is concluded that the existing CALPHAD databases are reliable for LPSO 14H prediction for the Mg–Gd–Y–Zn system, but more work is needed to improve the reliability of the other predicted phases.

Acknowledgements This work was funded by the Army Research Laboratory (ARL) and Terves LLC. The authors would like to acknowledge Dr. Vincent Hammond with ARL, Dr. William Meier of Oak Ridge National Laboratory, and the Light Metals and Manufacturing Laboratory members at The Ohio State University for their insightful discussions. This material is based upon the work supported by the Army Contracting Command—Adelphi, MD under Contract No W911QX-18-P-0038. Any opinions, findings, and conclusions or recommendations expressed in this material are those of the author(s) and do not necessarily reflect the views of ARL.

References

1. Abe E, Kawamura Y, Hayashi K, Inoue A (2002) Long-period ordered structure in a high-strength nanocrystalline Mg-1 at% Zn-2 at% Y alloy studied by atomic-resolution Z-contrast STEM. *Acta Mater* 50(15):3845–3857
2. Kawamura Y, Kasahara T, Izumi S, Yamasaki M (2006) Elevated temperature Mg₉₇Y₂Cu₁ alloy with long period ordered structure. *Scripta Mater* 55(5):453–456
3. Du XH, Duan GS, Hong M, Wang DP, Wu BL, Zhang YD, Esling C (2014) Effect of V on the microstructure and mechanical properties of Mg–10Er–2Cu alloy with a long period stacking ordered structure. *Mater Lett* 122:312–314
4. Bi GL, Li YD, Huang XF, Chen TJ, Lian JS, Jiang ZH, Ma Y, Hao Y (2015) Deformation behavior of an extruded Mg–Dy–Zn alloy with long period stacking ordered phase. *Mat Sci Eng A—Struct*, 622:52–60
5. Kawamura Y, Yamasaki M (2007) Formation and Mechanical Properties of Mg₉₇Zn₁RE₂ Alloys with Long-Period Stacking Ordered Structure. *Mater Trans* 48(11): 2986–2992
6. Datta A, Waghmare UV, Ramamurty U (2008) Structure and stacking faults in layered Mg–Zn–Y alloys: A first-principles study. *Acta Mater* 56(11): 2531–2539
7. Suzuki M, Kimura T, Koike J, Maruyama K (2003) Strengthening effect of Zn in heat resistant Mg–Y–Zn solid solution alloys. *Scripta Mater* 48(8):997–1002
8. Lu FM, Ma AB, Jiang JH, Yang DH, Zhou Q (2012) Review on long-period stacking-ordered structures in Mg–Zn–RE alloys. *Rare Metals* 31(3): 303–310
9. Kim JK, Jin L, Sandlöbes S, Raabe Dierk (2017) Diffusional-displacive transformation enables formation of long-period stacking order in magnesium. *Sci Rep-UK* <https://doi.org/10.1038/s41598-017-04343-y>
10. Xu D, Han EH, Xu YB (2016) Effect of long-period stacking ordered phase on microstructure, mechanical property and corrosion resistance of Mg alloys: A review. *Prog Nat Sci Mater* 26(2): 117–128
11. Wang K, Wang JF, Huang S, Gao SQ, Guo SF, Liu SJ, Chen XH, Pan FS (2018) Enhanced mechanical properties of Mg–Gd–Y–Zn–Mn alloy by tailoring the morphology of long period stacking ordered phase. *Mat Sci Eng A Struct* 733: 267–275
12. Zhang S, Yuan GY, Lu C, Ding WJ (2011) The relationship between (Mg,Zn)3RE phase and 14H-LPSO phase in Mg–Gd–Y–Zn–Zr alloys solidified at different cooling rates. *J Alloy Compd* 509(8): 3515–3521
13. Honma T, Ohkubo T, Kamado S, Hono K (2007) Effect of Zn additions on the age-hardening of Mg–2.0Gd–1.2Y–0.2Zr alloys. *Acta Mater* 55(12): 4137–4150
14. Yamada K, Okubo Y, Shiono M, Watanabe H, Kamado S, Kojima Y (2006) Alloy Development of High Toughness Mg–Gd–Y–Zn–Zr Alloys. *Mater Trans* 47(4):1066–1070
15. Shi F, Wang CQ, Guo XF (2015) Microstructures and Properties of As-Cast Mg₉₂Zn₄Y₄ and Mg₉₂Zn₄Y₃Gd₁ Alloys with LPSO Phase. *Rare Metal Mat Eng* 44(7): 1617–1622
16. Luo L, Liu Y, Duan M (2018) Phase Formation of Mg–Zn–Gd Alloys on the Mg-rich Corner. *Materials* 11(8): <https://doi.org/10.3390/ma11081351>
17. Hu YB, Zhang C, Zheng TX, Pan FS, Tang AT (2018) Strengthening Effects of Zn Addition on an Ultrahigh Ductility Mg–Gd–Zr Magnesium Alloy. *Materials* 11(10): <https://doi.org/10.3390/ma11101942>
18. Wen K, Liu K, Wang ZH, Li SB, Du WB (2016) Effect of pre-solution treatment on mechanical properties of as-extruded Mg_{96.9}Zn_{0.43}Gd_{2.48}Zr_{0.15} alloy. *Mat Sci Eng A Struct* 674: 33–39
19. Matsuda M, Ando A, Nishida M (2005) Dislocation Structure in Rapidly Solidified Mg₉₇Zn₁Y₂ Alloy with Long Period Stacking Order Phase. *Mater Trans* 46(2): 361–364
20. Luo AA (2015), Material Design and Development: from Classical Thermodynamics to CALPHAD and ICME Approaches. *CALPHAD*, 50: 6–22

21. Li YX, Yang CL, Zeng XQ, Jin PP, Qiu D, Ding WJ (2018) Microstructure evolution and mechanical properties of magnesium alloys containing long period stacking ordered phase. *Mater Charact* 141: 286–295
22. Itoi T, Seimiya T, Kawamura Y, Hirohashi M (2004) Long period stacking structures observed in Mg₉₇Zn₁Y₂ alloy. *Scripta Mater* 51 (2): 107–111
23. Zhu YM, Morton A, Nie JF (2012) Growth and transformation mechanisms of 18R and 14H in Mg–Y–Zn alloys. *Acta Mater* 60 (19): 6562–6572
24. Yamasaki M, Sasaki M, Nishijima M, Hiraga K, Kawamura Y (2007) Formation of 14H long period stacking ordered structure and profuse stacking faults in Mg–Zn–Gd alloys during isothermal aging at high temperature. *Acta Mater* 55(20): 6798–6805
25. Li B, Teng BG, Luo DG (2018) Effects of Passes on Microstructure Evolution and Mechanical Properties of Mg–Gd–Y–Zn–Zr Alloy During Multidirectional Forging. *Acta Metall Sin-Engl* 31 (10): 1009–1018
26. Yamasaki M, Anan T, Yoshimoto S, Kawamura Y (2005) Mechanical properties of warm-extruded Mg–Zn–Gd alloy with coherent 14H long periodic stacking ordered structure precipitate. *Scripta Mater* 53(7): 799–803
27. Wu J, Chiu YL, Jones IP (2014) Microstructure of as-cast Mg–4.2Zn–0.8Y (at.%) alloys containing Gd. *J Phys Conf Ser* 522: 8–12
28. Kishida K, Nagai K, Matsumoto A, Yasuhara A, Inui H (2015) Crystal structures of highly-ordered long-period stacking-ordered phases with 18R, 14H and 10H-type stacking sequences in the Mg–Zn–Y system. *Acta Mater* 99: 228–239
29. Garces G, Pérez P, Barea R, Medina J, Stark A, Schell N, Adeva P (2019) Increase in the Mechanical Strength of Mg–8Gd–3Y–1Zn Alloy Containing Long-Period Stacking Ordered Phases Using Equal Channel Angular Pressing Processing. *Metals* 9(2): <https://doi.org/10.3390/met9020221>
30. Zhang JY, Xu M, Teng XY, Zuo M (2016) Effect of Gd addition on microstructure and corrosion behaviors of Mg–Zn–Y alloy. *J Magnesium and Alloys* 4: 319–325
31. Wang K, W JF, Huang S, Gao SQ, Guo SF, Liu SJ, Chen XH, Pan FS (2018) Enhanced mechanical properties of Mg–Gd–Y–Zn–Mn alloy by tailoring the morphology of long period stacking ordered phase. *Mat Sci Eng A Struct* 33: 267–275